



HAL
open science

Bearing faults monitoring in electrical rotating machines through three-phase electrical signals analysis

Georgia Cablea, Pierre Granjon, Christophe Bérenguer

► **To cite this version:**

Georgia Cablea, Pierre Granjon, Christophe Bérenguer. Bearing faults monitoring in electrical rotating machines through three-phase electrical signals analysis. CM 2016 - MFPT 2016 - 13th International Conference on Condition Monitoring and Machinery Failure Prevention Technologies, Oct 2016, Paris, France. hal-01402872

HAL Id: hal-01402872

<https://hal.science/hal-01402872>

Submitted on 25 Nov 2016

HAL is a multi-disciplinary open access archive for the deposit and dissemination of scientific research documents, whether they are published or not. The documents may come from teaching and research institutions in France or abroad, or from public or private research centers.

L'archive ouverte pluridisciplinaire **HAL**, est destinée au dépôt et à la diffusion de documents scientifiques de niveau recherche, publiés ou non, émanant des établissements d'enseignement et de recherche français ou étrangers, des laboratoires publics ou privés.

Bearing faults monitoring in electrical rotating machines through three-phase electrical signals analysis

Georgia Cablea, Pierre Granjon and Christophe Bérenguer
Univ. Grenoble Alpes, GIPSA-lab, F-38000 Grenoble, France
CNRS, GIPSA-lab, F-38000 Grenoble, France

{georgia.cablea, pierre.granjon, christophe.berenguer}@gipsa-lab.grenoble-inp.fr

Abstract

Condition monitoring methods based on electrical signals analysis have been used for mechanical and electrical fault detection for a while now. Moreover, the research focus has shifted from single-phase signals analysis to three-phase signals approaches. The main advantages of using three-phase approaches can be stated as separation of balanced and unbalanced electrical quantities as well as better performances in terms of mechanical faults detection. However, such approaches still have a low industrial penetration in part due to their relatively higher complexity compared to single-phase approaches. The current paper proposes an easy to implement method for condition monitoring of bearings, which takes into account the whole three-phase electrical signals. After presenting the theoretical development of the method, the algorithm for computing mechanical faults indicators is given. Moreover, the paper presents experimental results of the proposed approach, using electrical signals acquired on a dedicated test bench.

1 Introduction

Three-phase rotating machines are used in a wide range of configurations of electro-mechanical systems for different industries. Thus, they are affected by both mechanical and electrical faults. In this paper the focus is set on the signature of mechanical faults in the three-phase electrical signals.

Models for mechanical faults signature in electrical signals have been developed throughout the years. A model for bearing fault signature was proposed in⁽¹⁾ based on the fact that such faults trigger air-gap eccentricities related to the faults. Such models have been later improved⁽²⁾ and it was shown that bearing faults may induce torque variations as well as eccentricity. Thus, they can trigger phase and/or amplitude modulations in the electrical signals at well defined frequencies for each case. Later the models were extended for any type of mechanical faults^(3,4), not just the bearings.

Methods to detect mechanical faults⁽⁴⁾ using electrical signals have initially focused on single phase stator currents and they are generically known as motor current signature analysis (MCSA)⁽⁵⁾. More recently the focus has shifted towards three-phase approaches. Most often these methods rely on the use of a three-phase transform, like the Fortescue transform⁽⁶⁾ or the Clarke/Concordia transform⁽⁷⁾, to combine the information in the three-phases and obtain the symmetrical components. Afterwards the obtained signals

are demodulated^(8,9,10,11,12) in order to study the presence of fault-related modulations. However, these demodulation techniques are based on the assumption that the obtained symmetrical components can be approximated to be an analytic signals which is not always the case.

Previous works⁽¹³⁾⁽¹⁴⁾ have proposed a method for condition monitoring of both mechanical and electrical faults that is based on correctly demodulating the symmetrical components corresponding to the electrical signals. The proposed method for mechanical fault detection is limited to modulations of frequencies lower than the fundamental frequency of the electrical signals. The current paper extends the approach to high-frequency modulations. The next section presents the proposed approach for mechanical faults detection. The section starts with the description of mechanical faults signatures in three-phase signals and then gives the proposed algorithm for obtaining mechanical fault indicators able to detect such faults. The third section of this article validates the proposed method using experimental signals acquired on a dedicated test bench. The last section of the article gives the conclusions and perspectives of the presented work.

2 Three-phase electrical signals analysis method for mechanical fault monitoring

In this section the content of electrical quantities in the presence of the signature of mechanical faults is presented. The expected behaviour of this signatures in the three-phase electrical signals is described and in the end mechanical fault indicators are proposed. Throughout the section the discussion is based on the three-phase currents. However, the same analysis can be performed on the voltages.

2.1 Mechanical fault signature in instantaneous symmetrical components

The instantaneous symmetrical components (ISCs) are obtained from the phase currents by applying the inverse Fortescue transform:

$$\begin{bmatrix} i_+(t) \\ i_-(t) \\ i_0(t) \end{bmatrix} = \frac{1}{3} \underbrace{\begin{bmatrix} 1 & a & a^2 \\ 1 & a^2 & a \\ 1 & 1 & 1 \end{bmatrix}}_{\mathbf{F}^{-1}} \begin{bmatrix} i_1(t) \\ i_2(t) \\ i_3(t) \end{bmatrix} \quad (1)$$

where $a = e^{j\frac{2\pi}{3}}$, \mathbf{F}^{-1} denotes the inverse of the Fortescue matrix⁽⁶⁾, and the ISCs of the original three-phase signal are: the positive-sequence ISC ($i_+(t)$), the negative-sequence ISC ($i_-(t)$) and the zero-sequence ISC ($i_0(t)$). In the rest of this paper, the transform defined in Equation (1) is referred to as ISC transform.

As long as the effects of the mechanical faults are present (torque variations and/or eccentricity) the fault signatures would be visible in the electrical quantities as modulations⁽²⁾. When comparing the value of the modulating frequency to the carrier frequency we can either have low-frequency modulations or high-frequency modulations. Figure 1 shows the expected signatures for both low-frequency modulations and high-frequency modu-

lations in ISCs for real-valued signals for which only the balanced components of the signals are modulated. There are three considerations that need to be made regarding this figure:

1. Firstly, there is a spectral redundancy in the ISCs. However, a full spectral analysis can be performed by only considering the modulations around $+f_0$ and this would be the case throughout the paper.
2. Secondly, if the negative-sequence ISC would also contain modulations, their amplitude would be really small. The amplitude of the modulations depends on the amplitude of the fundamental and for a functioning three-phase system, the amplitude of the negative-sequence ISC is very small. Thus, for mechanical faults detection throughout this paper, only the positive-sequence ISC would be considered.
3. Thirdly, the modulating frequency is assumed to be known. Indeed, this frequency can be easily determined using the kinematics of the system and the known operating conditions, like the rotating speed of the shaft. In the current paper, this frequency would be considered as an input of the algorithm.

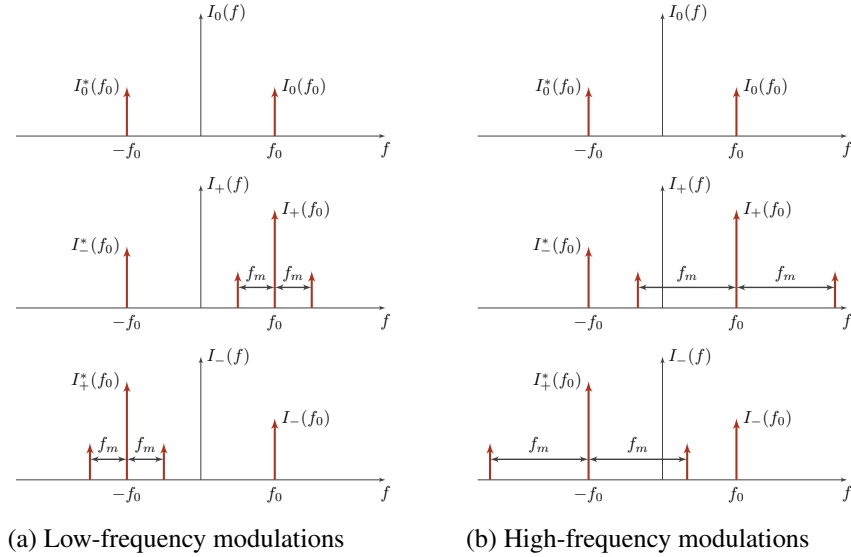


Figure 1: Frequency modulations in ISCs due to mechanical faults

Previous works^(13,14) have dealt with the case of low-frequency signatures of mechanical faults. An algorithm for extracting mechanical faults indicators by demodulating the electrical quantities has been proposed. The next section proposes an algorithm for the high-frequency case presented in Figure 1b. In this case, the modulating frequency is not negligible compared to the fundamental frequency. The algorithms will take into account the three-phase signal model as well as the previous observations. Thus, only modulations around the positive fundamental frequency $+f_0$ of the positive-sequence ISC will be analysed.

2.2 Algorithm for mechanical faults detection

The case of mechanical faults which have high-frequency signatures needs to be considered separately from the low-frequency one. Figure 1 depicts the two expected behaviours for these two cases. If the modulating frequency is higher than the fundamental frequency of the electrical quantities, as in Figure 1b, different aspects have to be taken into account:

1. The Hilbert demodulation technique previously used cannot be implemented as the necessary conditions are no longer fulfilled. In other words, the positive-sequence ISC cannot be assumed to be an analytic signal. For demodulated quantities of the positive-sequence ISC there was a single frequency band B centred around the fault characteristic frequency f_m considered for the fault indicator computation. For non-demodulated signals two frequency bands are to be considered B_l (the left-hand side band) and B_r (the right-hand side band). These bands will be centred around $f_0 \pm f_m$. Figure 2 graphically indicates the considered bands.
2. As the literature explains⁽¹⁵⁾ and the existing experimental data within the KAStrion project confirms, bearing faults characteristic frequency may vary by $\pm 2\%$. While for low-frequency faults this variation may be negligible, for high-frequency faults this aspect needs to be taken into account when computing the fault indicator. In case of really high frequencies, for example 200 Hz, this leads to a rather wide frequency band that needs to be considered, i.e. the corresponding band [196 204] Hz is 8 Hz wide.

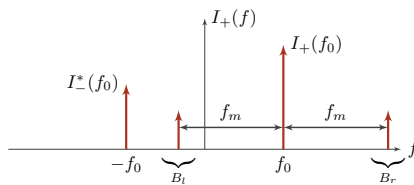


Figure 2: High-frequency modulation bands

The $\pm 2\%$ variation aspect is specific to bearing faults and the calculation of fault characteristic frequency bands for each possible mechanical fault is beyond the scope of this paper. However, what is important to consider is that the proposed algorithm for mechanical fault indicator computation must be robust with respect to the width of the fault characteristic frequency band.

Figure 3 gives the general structure of the algorithm for computing mechanical fault indicators for faults which have a high-frequency signature. This structure is very similar to the one proposed for the low-frequency mechanical faults indicators. This simplified version of the algorithm structure has removed the demodulation step and the PSD is estimated directly for the positive-sequence ISC. Afterwards, the fault indicator is computed considering the two corresponding frequency bands. The next sub-sections will give more details into the proposed indicators. Indeed, several indicators are to be computed, not just one. The following indicators are not assumed to be optimal. However they are easy to implement and remain efficient in detecting the eventual faults.

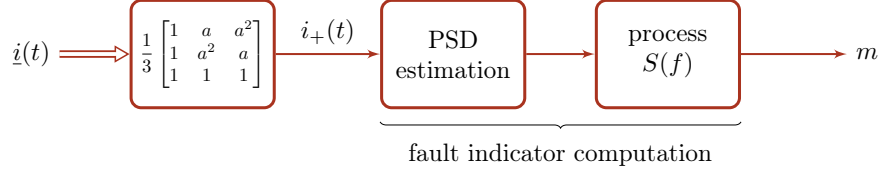


Figure 3: Structure of the algorithm for high-frequency mechanical fault indicators computation

2.2.1 Fault indicators based on the signal energy

Fault indicator 1 A mechanical fault indicator has been proposed in⁽¹⁴⁾ for mechanical faults inducing low-frequency modulations. The corresponding indicator is to be computed over a narrow frequency band using demodulated signals and is expressed as:

$$m = \frac{\int_{(B)} S(f) df}{\int_{(B)} S_h(f) df}, \quad (2)$$

where B denotes the considered frequency band, $S_h(f)$ denotes a reference PSD obtained for a healthy system and $S(f)$ is the current PSD.

This first indicator proposed for the high-frequency modulations is an extension of the indicator for low frequency given in Equation (2). Instead of considering just the frequency band B , both frequency bands (B_l and B_r) modulating the fundamental frequency f_0 are considered. The expression of this new indicator is given in (3).

$$m_1 = \frac{\int_{(B_l)} S(f) df + \int_{(B_r)} S(f) df}{\int_{(B_l)} S_h(f) df + \int_{(B_r)} S_h(f) df}, \quad (3)$$

where B_l and B_r denote the left and right frequency bands, $S_h(f)$ denotes a reference PSD obtained for a healthy system and $S(f)$ is the current PSD obtained for the system in an unknown state. In the case of an healthy condition, such an indicator stays obviously close to one, and tends to increase if faulty components appear in the signals.

In case of wide frequency bands (B_l and B_r), the contribution of two new peaks (one on each side) might be hard to detect in an incipient stage. Indeed, this indicator might not be sensitive enough to new peaks regardless of the frequency bands width.

Fault indicator 2 The second indicator proposed is an improvement of the first. Instead of using the whole energy in the given frequency bands B_l and B_r , the indicator can be computed using the amount of energy higher than the noise floor.

The first step in computing this indicator is to estimate the noise floor in each of the bands. The noise level can be estimated using a median filter over $S(f)$ for $f \in (B_l \cup B_r)$. The obtained estimations are denoted $S^n(f)$ and they only exist over B_l and B_r . Afterwards, a difference between the PSD $S(f)$ and the noise floor is computed. The quantity is denoted $S^d(f)$ and is obtained as:

$$S^d(f) = S(f) - S^n(f), \text{ for } f \in (B_l \cup B_r) \quad (4)$$

If the quantity $S^d(f)$ is greater than 0 then the current spectrum contains energy that is higher than the noise level. Thus, the proposed indicator only considers this amount of energy and is expressed as:

$$m_2 = \frac{\int_{(B_l \cup B_r)} S^d(f) \Big|_{S^d(f) > 0} df}{\int_{(B_l \cup B_r)} S_h^d(f) \Big|_{S_h^d(f) > 0} df}, \quad (5)$$

This indicator is normalised by the amount of energy computed for the healthy case.

2.2.2 Fault indicator based on frequency values

Fault indicator 3 The third proposed indicator uses the fact that there are two frequency bands that are symmetrical with respect to the fundamental frequency. In this case, a frequency will be obtained for each of the bands corresponding to the maximum difference between $S(f)$ and $S_h(f)$ in the given band. Thus, f_l corresponds to the frequency for which $(S(f) - S_h(f)) \Big|_{(B_l)}$ has the maximum value and consequently f_r denotes the frequency for which $(S(f) - S_h(f)) \Big|_{(B_r)}$ reaches maximum. The electrical fundamental frequency denoted f_0 corresponds to the maximum in $S(f)$. Considering that mechanical faults induce modulations, the interest is to determine whether the differences correspond to modulations. Thus, two new quantities are computed:

$$f_{m_l} = |f_l - f_0| \qquad f_{m_r} = |f_r - f_0| \quad (6)$$

Based on the two frequencies indicating the distance between the fundamental frequency and the frequencies of the maximal differences, a fault indicator is computed as:

$$m_3 = |f_{m_l} - f_{m_r}| \quad (7)$$

In case the two maxima differences correspond to a modulation of the fundamental frequency, the indicator m_3 would be null. A threshold can be set as the spectral resolution in order to ensure no detection is missed due to precision. In case the indicator is null, f_{m_l} and f_{m_r} indicate the modulating frequency itself.

This indicator is not very robust with respect to the content of the characteristic frequency bands. Indeed, it relies on the assumption that the modulation due to a mechanical fault represents the highest change with respect to the estimated healthy condition. This assumption is not necessarily true in all practical cases. For example one of the bands might present its highest change at a frequency location corresponding to a different modulation of a harmonic. The wider the bands the higher the chance is for them to also contain other components besides modulations of the fundamental frequency.

3 Experimental results

3.1 Experimental set-up

These indicators were tested using experimental data coming from a test-bench purposely designed and developed in the CETIM laboratory (Senlis, France)⁽¹⁶⁾. The bench emulates the structure and behaviour of a wind turbine, with an electrical motor replacing the wind turbine rotor, followed by a low speed shaft with the main bearing, a gearbox, high speed shaft and three-phase electrical generator. The operating conditions are determined by the speed of the low speed shaft. For the experiment considered in this paper a radial load force was applied on the output bearing (located on the high-speed shaft) leading to an accelerated deterioration of this bearing.

This experiment has run for ≈ 900 hours. At the end, the output bearing was dismantled and it was visually inspected. The visual inspection showed there was no flaking, but a distributed wear over half the outer race (remained smooth but cracked). There were also traces on the bore of the inner ring which show that this ring has rotated on the axis and therefore was not mounted sufficiently tight. Unfortunately, no pictures are available for this damaged bearing.

Table 1 gives the considered frequency band for the considered outer race fault, allowing 2% variations for ball-pass frequency - outer race (BPFO). The value for the BPFO was obtained using the kinematics of the system and the known rotating speed of the shaft. When analysing the electrical quantities the modulations will be expected in the left and right bands with respect to the fundamental frequency. Indeed, the bands of interest for the electrical quantities are located at $B_l = f_0 - \text{BPFOband}$ and $B_r = f_0 + \text{BPFOband}$.

Table 1: Fault characteristic frequency bands for Exp. B

LSS speed [rpm]	BPFO [Hz]	BPFO $\pm 2\%$ band [Hz]
20	223.03	[218.57 227.49]

3.2 Mechanical fault detection using electrical quantities

The computation of mechanical fault indicators is based on the estimated PSDs. For the considered experimental data the PSDs estimations are obtained with Welch averaged periodograms using a Hanning window of 2^{12} samples, leading to a spectral resolution of approximately 0.95 Hz. Indeed, the spectral resolution is rather poor. However, it was chosen accordingly because the fault indicator is computed over a wide frequency band and there is not a real interest in precisely detecting any given peak.

Figure 4 depicts a zoom in on the frequency bands of interest (the left-hand side band B_l and the right-hand side band B_r) in the PSDs of the current signal on phase 1 and the positive-sequence ISC. The figure shows that $i_+(t)$ has a better signal-to-noise ratio than the current $i_1(t)$. Also, after 350 hours into the experiment new peaks appear in these bands. This can be clearly seen in the PSD of $i_+(t)$ and it is less clear for $i_1(t)$.

Nonetheless, one of the datasets acquired after the 350 hours does not present any new peaks. The PSDs of the other two current signals are similar to that of $i_1(t)$.

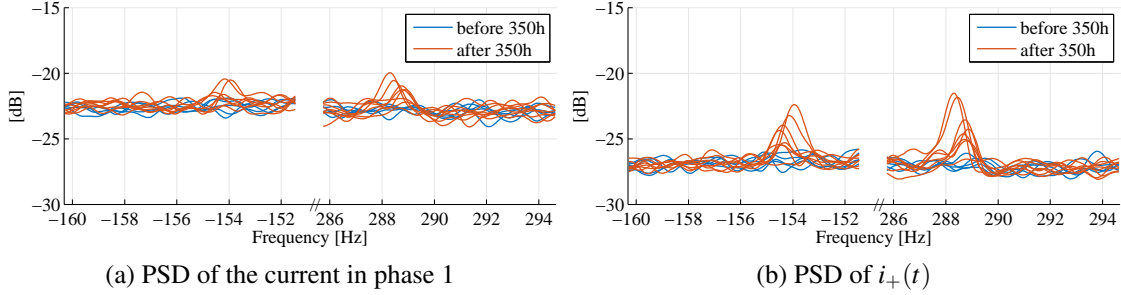


Figure 4: PSDs of the current signals

Based on the PSDs of the electrical signals in the frequency bands of interest, the mechanical fault indicators were computed. The indicators were computed for both currents and voltages, for the positive-sequence ISCs as well as for the phase signals by applying the same algorithm. This approach allows the comparison in terms of detection capabilities between single-phase and three-phase methods. For all indicators, the healthy case estimation S_h was considered to correspond to the first dataset acquired.

3.2.1 Fault indicators based on signal energy

Figure 5 depicts the results obtained for the first mechanical fault indicator denoted m_1 and expressed in (3). There are several aspects highlighted in this figure. Firstly, the indicators computed using positive-sequence ISCs provide better results than the ones using the single-phase quantities. The higher amplitudes of the indicator towards the end of the experiment are more clearly distinguishable from the lower values at the beginning. Secondly, the voltage signals provide better results than the current signals. This might be explained by the fact that the voltage signals have higher amplitudes than the currents around the fundamental, thus the amplitudes of the modulations are also higher. Another aspect contributing to this result is that for this test bench the generator output is not directly connected to the grid, thus its voltage amplitude and fundamental frequency is allowed to vary and are not imposed by the grid. Regarding the absence of the bearing fault signature in the signals acquired right before 800 hours, one possible reason could be the fact that the bearings were not tightly fixed. In this case the fault position might change with respect to the load area and this might lead to a difference or temporary absence of the signature.

All in all, using the indicator m_1 computed for $v_+(t)$ and by setting an correct threshold the signature of the mechanical fault can be detected from the beginning of its apparition. However, this indicator performs rather poorly when applied to all other signals. This was expected considering the wide band (2 times 8.92 Hz) over which it was computed. The contribution added by the two new peaks is small compared to the total sum over the ≈ 18 Hz.

The poor performance of the first indicator justifies the need for improvement, thus the

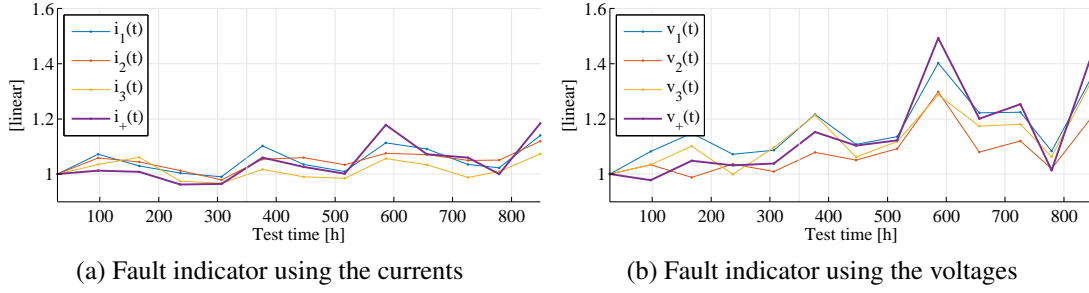


Figure 5: Mechanical fault indicator m_1 considering both left and right fault characteristic frequency bands

definition of the second indicator named m_2 given in Equation (5). The order of the median filter used to estimate the noise is set as five times the spectral resolution. Figure 6 explains how this indicator is computed by depicting the right-hand side modulation band B_r for the first and last $i_+(t)$. In this figure the median for each of these two PSDs is also depicted while the gray area indicates the quantities used to compute the indicator m_2 . For the first dataset, also considered healthy, the gray area is small. For the last dataset a new peak is visible and the gray area under it is large compared to the healthy case.

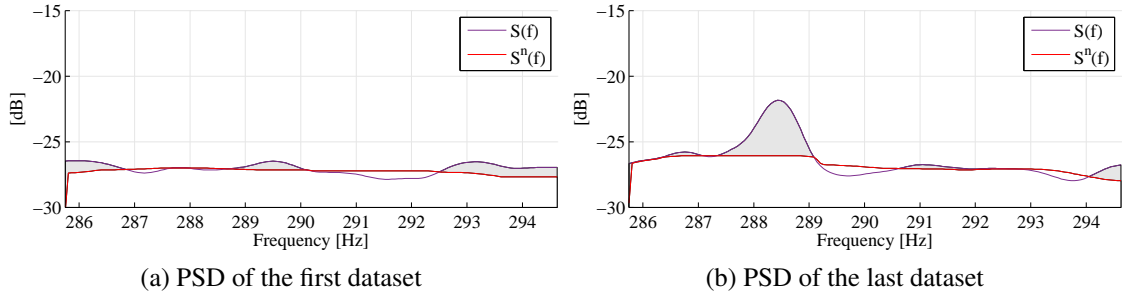


Figure 6: Right-hand side modulation band for $i_+(t)$

Figure 7 shows the mechanical fault indicator m_2 . The indicator computed using single-phase current signals is still not capable to clearly separate the values before and after the fault. This result is expected to be poor, considering for example the PSD of $i_1(t)$ presented in Figure 4 which shows that the phase signal has a poorer SNR than $i_+(t)$. More so, the modulations in the left-hand side band of the currents PSDs are not visible for most of the single-phase signals. The results provided by this indicator enables the detention of the fault starting before 400 hours using all voltage signals and the positive-sequence ISC for the currents.

3.2.2 Fault indicators based on frequency values

Figure 8 shows the frequencies for the maximum difference between each given PSD and the one that was estimated for the first dataset considered healthy. These frequency values pairs correspond to f_{ml} and f_{mr} from Equations (6). At the beginning of the experiment these values vary all over the frequency band which corresponds to the bearing outer race fault. After 350 hours the left and right frequency value both converge towards the same

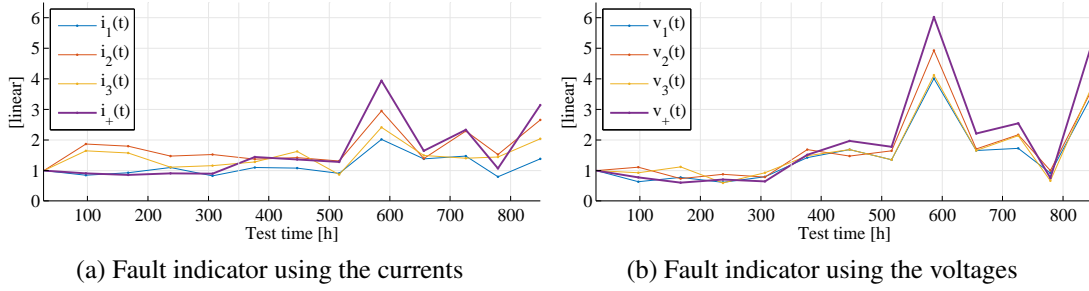


Figure 7: Mechanical fault indicator m_2

value for all the voltages and for $i_+(t)$. This suggests that the actual modulating frequency is between 221 and 222 Hz, and not precisely equal to the theoretical value of 223 Hz.

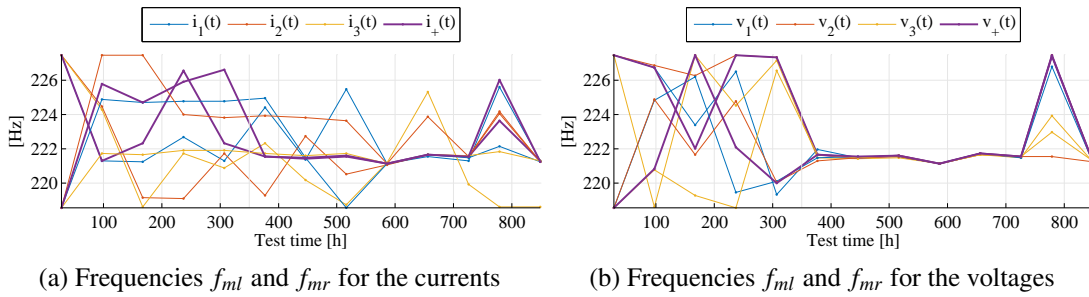


Figure 8: Frequencies for the maximum difference between the PSDs

Figure 9 shows the indicator m_3 obtained using the two above frequencies. If the value of this indicator is lower than the spectral resolution of 0.95 Hz the results suggests that there is a modulation of the fundamental frequency present in the frequency bands corresponding to BPFO. Thus this indicator is able to detect the appearance of the modulation using all three phase voltage signals as well as $v_+(t)$. Regarding the currents, the indicator can detect the presence of the modulation using $i_+(t)$ but the fault is still not properly detected using the single-phase currents.

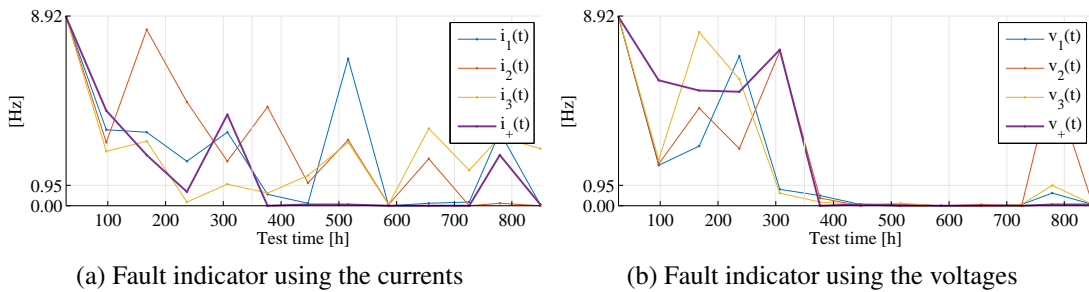


Figure 9: Mechanical fault indicator m_3

If only random noise is present in the corresponding bands the current algorithm still returns a frequency value for each band. Thus the probability of false alarm is rather high

in this case as randomly the maximum difference between the noises in the bands can falsely indicate a modulation as is the case for the value for $i_+(t)$ right after 200 hours. This indicator can be improved by only providing values for f_{ml} and f_{mr} when peaks are present.

4 Conclusions

In this paper a method for condition monitoring of mechanical components has been proposed. The method relies on the use of three-phase signals and more specifically their positive-sequence instantaneous symmetrical component. Using this quantity two kinds of mechanical fault indicators have been proposed based on the signal energy and on the frequency values of components located in the frequency bands corresponding to the faults. The proposed method has been validated using experimental results. Throughout the presentation of the experimental results the three-phase approach has been compared to the single-phase one showing that the use of the positive-sequence ISC is justified by its better performance in detecting mechanical faults. Indeed, the proposed mechanical fault indicators computed using the positive-sequence ISC were able to detect the outer race bearing fault that generated high-frequency modulations.

As future developments of this work, the mechanical fault indicator that relies on the frequency values can be further improved. By only computing the modulating frequency value for detected peaks the number of false alarms triggered by this indicator can be reduced.

Acknowledgements

This research has been partly supported by KIC InnoEnergy, a company supported by the European Institute of Innovation and Technology (EIT), through KAStrion European project.

The authors would like to thank CETIM (Centre Technique des Industries Mécaniques) for providing the test-bench and experimental data.

References

1. R. Schoen, T. Habetler, F. Kamran, and R. Bartfield, "Motor bearing damage detection using stator current monitoring," *IEEE Transactions on Industry Applications*, vol. 31, no. 6, pp. 1274–1279, Dec. 1995.
2. M. Blodt, P. Granjon, B. Raison, and G. Rostaing, "Models for Bearing Damage Detection in Induction Motors Using Stator Current Monitoring," *IEEE Transactions on Industrial Electronics*, vol. 55, no. 4, pp. 1813–1822, Apr. 2008.
3. M. Blodt, J. Regnier, and J. Faucher, "Distinguishing load torque oscillations and eccentricity faults in induction motors using stator current wigner distributions," *IEEE Transactions on Industry Applications*, vol. 45, no. 6, pp. 1991–2000, 2009.

4. M. Blodt, P. Granjon, B. Raison, and J. Regnier, "Mechanical fault detection in induction motor drives through stator current monitoring - theory and application examples," in *Fault Detection*, W. Zhang, Ed. InTech, 2010, pp. 451–487.
5. H. A. Toliyat, S. Nandi, S. Choi, and H. Meshgin-Kelk, Eds., *Electric machines: modeling, condition monitoring, and fault diagnosis*. CRC Press, 2013.
6. C. L. Fortescue, "Method of symmetrical co-ordinates applied to the solution of polyphase networks," *Transactions of the American Institute of Electrical Engineers*, vol. XXXVII, no. 2, pp. 1027–1140, July 1918.
7. E. Clarke, *Circuit Analysis of A-C Power Systems*. New York : J. Wiley & Sons, Inc., 1943.
8. J. L. H. Silva and A. J. M. Cardoso, "Bearing failures diagnosis in three-phase induction motors by extended Park's vector approach," in *31st Annual Conference of IEEE Industrial Electronics Society, 2005. IECON 2005.*, Nov 2005, pp. 6 pp.–.
9. B. Trajin, M. Chabert, J. Regnier, and J. Faucher, "Hilbert versus Concordia transform for three-phase machine stator current time-frequency monitoring," *Mechanical Systems and Signal Processing*, vol. 23, no. 8, pp. 2648–2657, Nov. 2009.
10. Y. Amirat, V. Choqueuse, and M. E. H. Benbouzid, "Wind turbines condition monitoring and fault diagnosis using generator current amplitude demodulation," in *Energy Conference and Exhibition (EnergyCon), 2010 IEEE International*, Dec 2010, pp. 310–315.
11. V. Choqueuse, M. E. H. Benbouzid, Y. Amirat, and S. Turri, "Diagnosis of three-phase electrical machines using multidimensional demodulation techniques," *IEEE Transactions on Industrial Electronics*, vol. 59, no. 4, pp. 2014–2023, 2012-04.
12. E. H. El Bouchikhi, V. Choqueuse, M. Benbouzid, and J. A. Antonino-Daviu, "Stator current demodulation for induction machine rotor faults diagnosis," in *Green Energy, 2014 International Conference on*, March 2014, pp. 176–181.
13. G. Cablea, P. Granjon, and C. Bérenguer, "Method for computing efficient electrical indicators for offshore wind turbine monitoring," *Insight - Non-Destructive Testing and Condition Monitoring*, vol. 56, no. 8, pp. 443–448, Aug 2014.
14. G. Cablea, P. Granjon, C. Bérenguer, and P. Bellemain, "Online condition monitoring of wind turbines through three-phase electrical signature analysis," in *CD proceedings of the Twelfth International Conference on Condition Monitoring and Machinery Failure Prevention Technologies*, June 2015.
15. R. B. Randall and J. Antoni, "Rolling element bearing diagnostics—A tutorial," *Mechanical Systems and Signal Processing*, vol. 25, no. 2, pp. 485–520, Feb. 2011.
16. N. Bédouin and S. Sieg-Zieba, "Endurance testing on a wind turbine test bench. A focus on slow rotating bearing monitoring," in *CD proceedings of the Twelfth International Conference on Condition Monitoring and Machinery Failure Prevention Technologies*, June 2015.